2011 American Control Conference
on O'Farrell Street, San Francisco, CA, USA
June 29 - July 01, 2011

# Robust H$^\infty$ control in fast Atomic Force Microscopy *

Ning Chuang, Ian R. Petersen and Himanshu R. Pota **

***Abstract*— This paper presents the design of a robust $H^\infty$ controller for fast tracking of an Atomic Force Microscope (AFM). The controller design is based on a physical model of the AFM piezoelectric tube positioner. External capacitors are connected in series with the x and y contacts of the piezoelectric tube to provide measured voltages which are proportional to the charge on the actuator. The parameters for a nonlinear hysteresis model are obtained from measurements of the system frequency response and time domain response. Experimental results show that the robust $H^\infty$ controller can increase the scanning speed significantly.**

## I. Introduction

This paper describes an approach to controlling the scanning stage in an Atomic Force Microscope, see Figure 1. In recent years, there has been large amount of research interest in tracking control problems for probe-based imaging and nano-positioning; e.g. see [1]. A variety of different control methods have been developed to control piezoelectric positioning devices to generate controlled motion with fast positioning. The most typical and traditional control method is the PID method such as used in the commercial NT-MDT Ntegra scanning probe microscope (SPM).

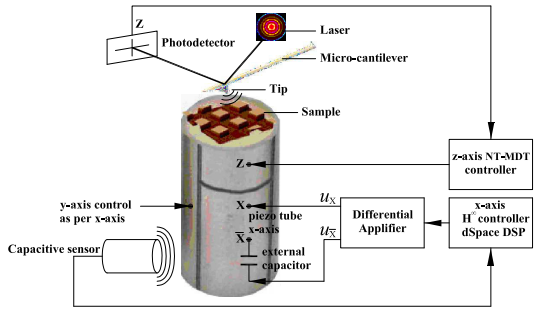


Fig. 1. Robust $H^\infty$ controller connection on the AFM

Many previous papers have dealt with the tracking control problems arising in such nano-positioning problems; e.g., see [1]–[9], [11]–[13], [15]. The features of our controller design method as compared to these previous approaches are as follows: we treat the nonlinear hysteresis in the AFM piezoelectric actuator as a sector bounded nonlinearity; we use an external capacitor connected in series with the piezoelectric actuator to provide an extra measurement which leads to a similar effect as the charge-controlled method of [14]; we use a robust $H^\infty$ tracking control approach to synthesize the controller taking into account the resonant nature of the system being controlled. The Atomic Force Microscope being considered is an NT-MDT Ntegra SPM system. It is required that the displacement of the scanner tracks a sawtooth reference input signal. Our motivation is to increase the AFM scanning speed with improved quality in the scanned images when compared with the existing AFM internal PID controller.

## II. The AFM system model

Our model for the AFM piezoelectric actuator is similar to that used in [23] and [24], based on the model given in [16] which uses a description consisting of both electrical and mechanical elements, see Figure 2. An expression [16] for the relationship between the interaction force $F_P$ generated by the actuator and the voltages $U_h$ and $U_P$ in this model is

$$F_P = T_{em}(U_h + U_P). \tag{1}$$

In equation (1), $T_{em}$ is defined as the transformer ratio between the electrical energy and mechanical energy of the piezoelectric actuator of the AFM.

We consider the electrical model of a piezoelectric actuator discussed in [16], [23] and [24] which is similar to the actuator used in the AFM system, except that the actuator in this paper is a piezoelectric tube. This electrical model is shown in Figure 2.

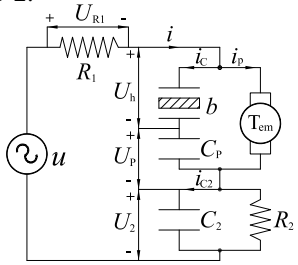


Fig. 2. An electrical circuit model of the electrical side of the piezoelectric tube actuator.

Here $u$ represents the amplifier voltage applied to the circuit, $R_1$ represents the output resistance of the amplifier driving the actuator, $C_2$ is the capacitance of an external capacitor in series with the piezoelectric actuator, $U_2$ is the voltage across the external capacitor, which is measured using a differential probe, $R_2$ is the equivalent resistance of the differential probe. In the papers [16], [23] and [24], a nonlinear model is proposed for the relationship between the hysteresis voltage $U_h$ and the charge $q$. This is described by the equation:

$$\dot{q} = \alpha|\dot{U}_h|(a\ U_h - q) + b\ \dot{U}_h \tag{2}$$

where $\alpha > 0$, $a > 0$ and $b > 0$ are constants which determine the size and shape of the hysteresis nonlinearity. If $\alpha$ is small, the system can be considered as being approximately linear. Using (2), a nonlinear relationship between the current $i$ in the piezoelectric actuator and the derivative of the voltage generated by the hysteresis, $\dot{U}_h$ can be derived as follows:

$$\dot{q} = i = \begin{cases} (b + \alpha(a\,U_h - q))\,\dot{U}_h & \text{if } \dot{U}_h \geq 0; \\ (b - \alpha(a\,U_h - q))\,\dot{U}_h & \text{if } \dot{U}_h < 0. \end{cases} \tag{3}$$

*This work was supported by the Australian Research Council.

** Ning Chuang, Ian R. Petersen and Himanshu R. Pota are with the School of Engineering and Information Technology, University of New South Wales at the Australian Defence Force Academy, Canberra ACT 2600, Australia. ning1@tpg.com.au; i.r.petersen@gmail.com; h.pota@adfa.edu.au.

This relationship is presented graphically in Figure 3.

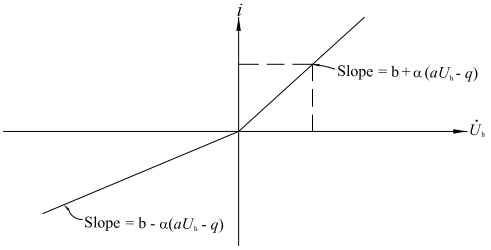


Fig. 3. Graph of the relationship between $i$ and $\dot{U}_h$.

From Figure 3, it is clear that the function $i = g(\dot{U}_h)$ defined in (3) has an inverse provided $|q - a\,U_h| \leq \frac{b}{\alpha}$. This inverse function is as follows:

$$\dot{U}_h = f(i) = \begin{cases} \frac{i}{b+\alpha(aU_h - q)} & \text{if } i \geq 0; \\ \frac{i}{b-\alpha(aU_h - q)} & \text{if } i < 0. \end{cases} \quad (4)$$

From equations (1) and (4), we can use the circuit shown in Figure 2 to derive a state space model of the AFM piezoelectric tube actuator.

To determine a model for the mechanical side of AFM positioning system, we obtained frequency response measurements that showed the system has two closely spaced mechanical resonances. Hence, we assume that the transfer function of the mechanical subsystem from force input to displacement output is as follows:

$$\frac{d(s)}{F_P(s)} = \frac{K_1 \frac{1}{m_1}}{s^2 + \frac{c_1}{m_1}s + \frac{k_1}{m_1}K_1} + \frac{K_2 \frac{1}{m_2}}{s^2 + \frac{c_2}{m_2}s + \frac{k_2}{m_2}K_2}. \quad (5)$$

From the measured AFM displacement frequency response, there are two resonant peaks located closely at $\omega_1$ and $\omega_2$ respectively. Hence, the displacement of the actuator $d$ is then defined as $K_1 d_1 + K_2 d_2$ in order to make the model well matched, where $K_1$ and $K_2$ are constants given by the opposite signs and $d_1$ and $d_2$ are proportional to the one part of the total displacement according to the two resonance. This leads us to define the state variables $x_1 = K_1 d_1$, $x_2 = \frac{\dot{d}_1}{K_1}$, $x_3 = K_2 d_2$, $x_4 = \frac{\dot{d}_2}{K_2}$, $x_5 = U_2$, $x_6 = U_h$, $x_7 = U_P$ and $x_8 = q$. The state equations for $x_1$, $x_2$, $x_3$ and $x_4$ can be obtained from the terms in the transfer functions in (5). Also, the state equation for $x_5 = U_2$ can be derived from the fact that by $i_{C_2} = \dot{U}_2 C_2 = \frac{U_{R1}}{R_1} - \frac{U_2}{R_2}$. Furthermore, the state equations for $x_6$ and $x_8$, which contain the nonlinear relationship between $q$ and $U_h$, are obtained from (4) and Kirchhoff's Laws to obtain an expression for $i$. The state equation for $x_7$ is derived from the equation $q_p = T_{em}\, y$ which is given in the paper [16]. Here $\dot{q}_p = i_p$ as shown in Figure 2. This leads to the equation $\dot{q}_p = T_{em}\,\dot{y} = i - C_P\,\dot{U}_p$. Thus, a complete state space model for the AFM positioning system can be written as follows:

$$\begin{aligned}
\dot{x}_1 &= K_1 x_2; \\
\dot{x}_2 &= -\tfrac{k_1}{m_1}x_1 - \tfrac{c_1}{m_1}x_2 + \tfrac{T_{em}}{m_1}x_6 + \tfrac{T_{em}}{m_1}x_7; \\
\dot{x}_3 &= K_2 x_4; \\
\dot{x}_4 &= -\tfrac{k_2}{m_2}x_3 - \tfrac{c_2}{m_2}x_4 + \tfrac{T_{em}}{m_2}x_6 + \tfrac{T_{em}}{m_2}x_7; \\
\dot{x}_5 &= -(\tfrac{1}{R_1C_2} + \tfrac{1}{R_2C_2})x_5 - \tfrac{1}{R_1C_2}x_6 - \tfrac{1}{R_1C_2}x_7 + \tfrac{1}{R_1C_2}u; \\
\dot{x}_6 &= \begin{cases} \frac{-T_{em}x_2 - T_{em}x_4 - \frac{1}{R_1}x_5 - \frac{1}{R_1}x_6 - \frac{1}{R_1}x_7 + \frac{1}{R_1}u}{b + \alpha(ax_6 - x_8)} & \text{if } i \geq 0; \\ \frac{-T_{em}x_2 - T_{em}x_4 - \frac{1}{R_1}x_5 - \frac{1}{R_1}x_6 - \frac{1}{R_1}x_7 + \frac{1}{R_1}u}{b - \alpha(ax_6 - x_8)} & \text{if } i < 0; \end{cases} \\
\dot{x}_7 &= -\tfrac{T_{em}}{C_P}x_2 - \tfrac{T_{em}}{C_P}x_4 - \tfrac{1}{R_1C_P}x_5 - \tfrac{1}{R_1C_P}x_6 - \tfrac{1}{R_1C_P}x_7 + \tfrac{1}{R_1C_P}u; \\
\dot{x}_8 &= -\tfrac{1}{R_1}x_5 - \tfrac{1}{R_1}x_6 - \tfrac{1}{R_1}x_7 + \tfrac{1}{R_1}u; \\
y &= \begin{bmatrix} d \\ U_2 \end{bmatrix}. \quad (6)
\end{aligned}$$

The eighth-order nonlinear state space model (6) can be used to simulate the nonlinear dynamics of the AFM positioning system. In order to determine the parameters in this model, both time and frequency domain measurements were made on the experimental system. The two measured outputs of the AFM positioning system are specified as the displacement $d$ and the series capacitor voltage $U_2$.

For the displacement $d$ sensor output, an additional transfer function combining a low-pass filter and a time delay is added to the position output of the model to allow for the time delay arising from the capacitive sensor electronics. The value of this delay time was determined to fit the measured frequency response data. The transfer function used to model this delay is a first order transfer function of the form:

$$T_d(s) = K_s\,\frac{\frac{\tau}{2}s - 1}{\frac{\tau}{2}s + 1}.$$

The corresponding low pass filter transfer function is of the form:

$$F(s) = \frac{1}{\frac{1}{P_s}s + 1}.$$

Here, the parameter $K_s$ represents the gain constant of the capacitive sensor electronics and $\tau$ is the sensor electronics time delay. Thus, $T(s) = T_d(s)\,F(s)$ is the transfer function from the displacement $d$ to the capacitive sensor output. A state space model for this transfer function is as follows:

$$\begin{aligned}
\dot{x}_d &= A_d\,x_d + B_d\,d; \\
\widetilde{d} &= C_d\,x_d + D_d\,d. \quad (7)
\end{aligned}$$

Here $\widetilde{d}$ denotes the position sensor output signal. Similarly, an additional time delay is also added to the output $U_2$ due to the fact that the measured value of $U_2$ is obtained through a signal access module and measured using a high voltage probe. This delay is also modeled as a first order transfer function of the form:

$$T_{U_2}(s) = \frac{\frac{\tau_2}{2}s - 1}{\frac{\tau_2}{2}s + 1}.$$

A state space model of this transfer function is as follows:

$$\begin{aligned}
\dot{x}_{d2} &= A_{d2}\,x_{d2} + B_{d2}\,U_2; \\
\widetilde{U}_2 &= C_{d2}\,x_{d2} + D_{d2}\,U_2. \quad (8)
\end{aligned}$$

To compare the model and measured frequency response, we first obtain state equations for a linear model derives from equation (6) by setting $\alpha = 0$:

$$\dot{x} = \begin{bmatrix}
0 & K_1 & 0 & 0 & 0 & 0 & 0 & 0 \\
\frac{-k_1}{m_1} & \frac{-c_1}{m_1} & 0 & 0 & 0 & \frac{T_{em}}{m_1} & \frac{T_{em}}{m_1} & 0 \\
0 & 0 & 0 & K_2 & 0 & 0 & 0 & 0 \\
0 & 0 & \frac{-k_2}{m_2} & \frac{-c_2}{m_2} & 0 & \frac{T_{em}}{m_2} & \frac{T_{em}}{m_2} & 0 \\
0 & 0 & 0 & 0 & \frac{-R_2-R_1}{R_1R_2C_2} & \frac{-1}{R_1C_2} & \frac{-1}{R_1C_2} & 0 \\
0 & \frac{-T_{em}}{b} & 0 & \frac{-T_{em}}{b} & \frac{-1}{R_1 b} & \frac{-1}{R_1 b} & \frac{-1}{R_1 b} & 0 \\
0 & \frac{-T_{em}}{C_P} & 0 & \frac{-T_{em}}{C_P} & \frac{-1}{R_1 C_P} & \frac{-1}{R_1 C_P} & \frac{-1}{R_1 C_P} & 0 \\
0 & 0 & 0 & 0 & \frac{-1}{R_1} & \frac{-1}{R_1} & \frac{-1}{R_1} & 0
\end{bmatrix} x$$

$$+\begin{bmatrix} 0 \\ 0 \\ 0 \\ \frac{1}{R_1 C_2} \\ \frac{1}{R_1 b} \\ \frac{1}{R_1 C_P} \\ \frac{1}{R_1} \end{bmatrix} u; \quad y = \begin{bmatrix} K_S & 0 & K_S & 0 & 0 & 0 & 0 & 0 \\ 0 & 0 & 0 & 0 & K_{U_2} & 0 & 0 & 0 \end{bmatrix} x + \begin{bmatrix} D_d \\ D_{U_2} \end{bmatrix} u. \quad \text{Here,} \quad y = \begin{bmatrix} d \\ U_2 \end{bmatrix}. \tag{9}$$

Also, $K_S$ and $K_{U_2}$ are defined as the sensor gain and voltage gain due to the differential probe and the amplifier. $D_d$ and $D_{U_2}$ are defined as the DC offset values due to the scanned sample setup position. This gives a linear state space model of the form:

$$\begin{aligned} \dot{x} &= Ax + B\,u; \\ y &= Cx + D\,u. \end{aligned}$$

This state space model is augmented with the state equations (7) and (8) to give an overall linear state space model whose parameters will be chosen to fit the experimental measured frequency responses.

## III. Model Parameters

Frequency response tests showed the same frequency responses for both x and y directions of the AFM positioning system. This means that the same robust $H^\infty$ controller could be used for both the x and y directions. The experimentally measured frequency response data was obtained using an HP 35665A Dynamic Signal Analyzer (DSA), in which the DSA provided a source sinusoidal signal via a differential amplifier to the AFM piezoelectric tube. Thus, the outputs from the displacement $\widetilde{d}$ from the displacement capacitive sensor and the external capacitor voltage $\widetilde{U}_2$ were measured to plot the frequency response curves shown in Figures (4) and (5) respectively.

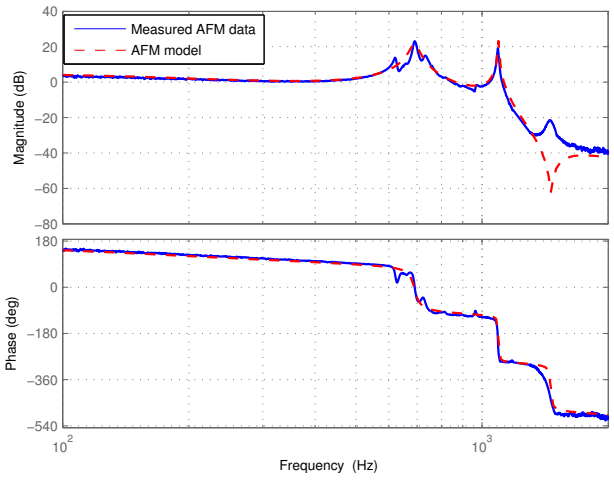


Fig. 4. Measured and model frequency responses for the transfer function from $u$ to $\widetilde{d}$ of the AFM positioning system.

The parameters in the linear system model (7), (8) and (9) were chosen to give a good match between the model frequency response and the measured frequency response. The model parameter values obtained are shown in Table I.

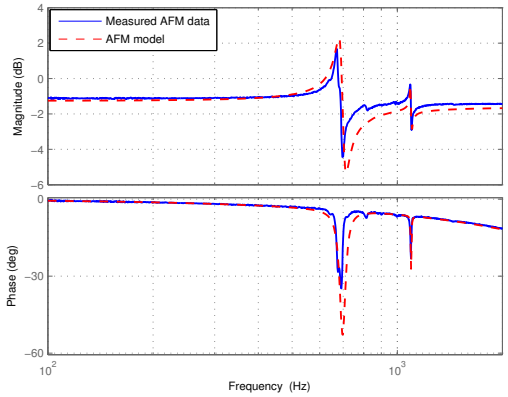


Fig. 5. Measured and model frequency responses for the transfer function from $u$ to $\widetilde{U}_2$ of the AFM positioning system.

| | |
|---|---|
| $b$ | $4.5 \times 10^{-7}$ F |
| $R_1$ | 50 Ω |
| $R_2$ | $2 \times 10^{9}$ Ω |
| $C_P$ | $4 \times 10^{-7}$ F |
| $C_2$ | $1 \times 10^{-8}$ F |
| $C_T$ | $2.12 \times 10^{-7}$ F |
| $T_{em}$ | $1 \times 10^{-2}$ C/m |
| $c_1$ | $2 \times 10^{-2}$ Ns/m |
| $c_2$ | $4.5 \times 10^{-3}$ Ns/m |
| $k_1$ | $3.943 \times 10^{3}$ N/m |
| $k_2$ | $9.1985 \times 10^{-18}$ N/m |
| $m_1$ | $6 \times 10^{-4}$ kg |
| $m_2$ | $2.33 \times 10^{-5}$ kg |
| $K_1$ | 7 |
| $K_2$ | −0.6 |
| $K_S$ | $-4.8 \times 10^{5}$ V/m |
| $K_{U_2}$ | −0.775 |
| $D_d$ | $-4 \times 10^{-8}$ |
| $D_{U_2}$ | −0.09 |
| $\tau$ | $8 \times 10^{-5}$ s |
| $\tau_2$ | $1.6 \times 10^{-5}$ s |

Table I Model parameter values.

## IV. Design of the Robust $H^\infty$ Controller

### A. Uncertain linear system model

In this paper, we apply a similar method to [23] and [24] involving sector bounded nonlinearities to solve a nonlinear tracking problem in the piezo-actuator based AFM positioning system.

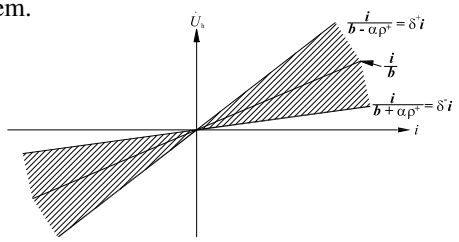


Fig. 6. Sector bounded nonlinearity in the piezoelectric actuator model.

A sector bound on the hysteresis nonlinearity (4) in our model is defined by the lines $\dot{U}_h = \delta^+ i$ and $\dot{U}_h = \delta^- i$, as shown in Figure 6. Here $\delta^+ > \delta^- > 0$. The corresponding sector bound is defined by the lines $\dot{U}_h = \delta^+ i$ and $\dot{U}_h = \delta^- i$, as shown in Figure 6. Here $\delta^+ > \delta^- > 0$, $\delta^+ = \frac{1}{b-\alpha\,\rho^+}$, $\delta^- = \frac{1}{b+\alpha\,\rho^+}$, $\delta^+ = \frac{1}{b-\alpha\,\rho^+}$ and $\delta^- = \frac{1}{b+\alpha\,\rho^+}$. Also, $\rho^+$ is the maximum value of $\rho = a\,U_h - q$.

In our case, a value of $\rho^+ = 8.22 \times 10^{-8}$ was used based on simulation of the nonlinear model (6). Thus, the

nonlinear equation (4) can be considered as a sector bounded nonlinearity if there is an upper bound on the magnitude of the quantity $\rho = a\,U_h - q$. This sector bounded nonlinearity can then be replaced by a norm bounded time-varying uncertainty.

Our approach to design a robust controller for the AFM positioning system in either the x direction control or y direction control involves a method of robust $H^\infty$ control with norm-bounded time-varying uncertainty via output feedback using the approach of [17] and [18]. This method for designing a robust $H^\infty$ controller was also used in [23] and [24]. In order to treat the sector bounded nonlinearity as a norm bounded uncertainty of the form considered in [17] and [18], we let the uncertainty be of the form: $f(i) = (\Delta_\delta \Delta(x) + \frac{1}{b})\dot{i}$; where $i = \dot{q}$ is defined in (6) and $\|\Delta(x)\| \leq 1$. Here,

$$\delta_o = \frac{\delta^+ + \delta^-}{2} \quad \text{and} \quad \Delta_\delta = \frac{\delta^+ - \delta^-}{2}.$$

This gives $\delta^+ = \delta_o + \Delta_\delta$ and $\delta^- = \delta_o - \Delta_\delta$. We have the following equation for the current $i$ in the actuator from (6):

$$\dot{q} = i = -\tfrac{1}{R_1}x_5 - \tfrac{1}{R_1}x_6 - \tfrac{1}{R_1}x_7 + \tfrac{1}{R_1}U.$$

Then, the state equation for $x_6$ becomes;

$$\begin{aligned}\dot{x}_6 \;=\; & -\tfrac{T_{em}}{b}x_2 - \tfrac{T_{em}}{b}x_4 - \tfrac{1}{R_1 b}x_5 - \tfrac{1}{R_1 b}x_6 - \tfrac{1}{R_1 b}x_7 + \tfrac{1}{R_1 b}U \\ & + \Delta_\delta \Delta(x)(E_1 x + E_2 u). \end{aligned} \tag{10}$$

$$\text{where} \quad \begin{aligned} E_1 &= \begin{bmatrix} 0 & 0 & 0 & 0 & -\frac{1}{R_1} & -\frac{1}{R_1} & -\frac{1}{R_1} \end{bmatrix}; \\ E_2 &= \begin{bmatrix} \frac{1}{R_1} \end{bmatrix}. \end{aligned}$$

Hence, this gives us an uncertain system of the form considered in [18]. Here, the term $\Delta_\delta \Delta(x)(E_1 x + E_2 u)$ can be regarded as providing a norm bounded perturbation to the linear state equation for $x_6$. The uncertain system model can be further simplified to decouple the state $x_8$ from all other state variables, as the state $x_8$ is defined as the current $i$ in the piezoelectric actuator. Then, the uncertain system model can be written as follows:

$$\dot{x} = \begin{bmatrix} 0 & K_1 & 0 & 0 & 0 & 0 & 0 \\ \frac{-k_1}{m_1} & \frac{-c_1}{m_1} & 0 & 0 & 0 & \frac{T_{em}}{m_1} & \frac{T_{em}}{m_1} \\ 0 & 0 & 0 & K_2 & 0 & 0 & 0 \\ 0 & 0 & \frac{-k_2}{m_2} & \frac{-c_2}{m_2} & 0 & \frac{T_{em}}{m_2} & \frac{T_{em}}{m_2} \\ 0 & 0 & 0 & 0 & \frac{-R_2-R_1}{R_1 R_2 C_2} & \frac{-1}{R_1 C_2} & \frac{-1}{R_1 C_2} \\ 0 & \frac{-T_{em}}{b} & 0 & \frac{-T_{em}}{b} & \frac{-1}{R_1 b} & \frac{-1}{R_1 b} & \frac{-1}{R_1 b} \\ 0 & \frac{-T_{em}}{C_P} & 0 & \frac{-T_{em}}{C_P} & \frac{-1}{R_1 C_P} & \frac{-1}{R_1 C_P} & \frac{-1}{R_1 C_P} \\ 0 & 0 & 0 & 0 & \frac{-1}{R_1} & \frac{-1}{R_1} & \frac{-1}{R_1} \end{bmatrix} x$$
$$+ \begin{bmatrix} 0 \\ 0 \\ \frac{1}{R_1 C_2} \\ \frac{1}{R_1 b} \\ \frac{1}{R_1 C_P} \end{bmatrix} u + \begin{bmatrix} \Delta A & \Delta B \end{bmatrix} \begin{bmatrix} x \\ u \end{bmatrix}$$

$$y = \begin{bmatrix} 1 & 0 & 1 & 0 & 0 & 0 & 0 \\ 0 & 0 & 0 & 0 & 1 & 0 & 0 \end{bmatrix} x = Cx. \tag{11}$$

$$\text{Here,} \quad \begin{bmatrix} \Delta A & \Delta B \end{bmatrix} \begin{bmatrix} x \\ u \end{bmatrix} = H_1\, \Delta(x)[E_1 x + E_2 u] = H_1 \xi \tag{12}$$

where $\xi = \Delta(x)\zeta$, $\zeta = i = E_1 x + E_2 u$, $\|\Delta(x)\| \leq 1$ and $H_1 = \begin{bmatrix} 0 & \Delta_\delta & 0 \end{bmatrix}^T$. Then, the uncertain system model (11), (12) can be rewritten as:

$$\begin{aligned} \dot{x} &= Ax + \begin{bmatrix} H_1 & B_2 \end{bmatrix} \begin{bmatrix} \xi \\ u \end{bmatrix}; \\ \begin{bmatrix} \zeta \\ \tilde{y} \end{bmatrix} &= \begin{bmatrix} E_1 \\ C \end{bmatrix} x + \begin{bmatrix} 0 & E_2 \\ 0 & 0 \end{bmatrix} \begin{bmatrix} \xi \\ u \end{bmatrix} \end{aligned} \tag{13}$$

where $\xi = \Delta(x)\,\zeta$ and $\|\Delta(x)\| \leq 1$.

We also simplify the model state equations (13) using a corresponding minimal realization to obtain the following equivalent uncertain system model:

$$\begin{aligned} \dot{x}_r &= A_r x_r + \begin{bmatrix} H_{1r} & B_{2r} \end{bmatrix} \begin{bmatrix} \xi \\ u \end{bmatrix}; \\ \begin{bmatrix} \zeta \\ d \\ U_2 \end{bmatrix} &= \begin{bmatrix} E_{1r} \\ C_{1r} \\ C_{2r} \end{bmatrix} x_r + \begin{bmatrix} H_{2r} & E_{2r} \\ H_{3r} & E_{3r} \\ H_{4r} & E_{4r} \end{bmatrix} \begin{bmatrix} \xi \\ u \end{bmatrix} \end{aligned} \tag{14}$$

where $\xi = \Delta(x)\,\zeta$ and $\|\Delta(x)\| \leq 1$.

### *B. Robust $H^\infty$ control problem formulation*

In order to obtain an uncertain system model on which the robust $H^\infty$ controller will be used, the state equations (14) are then augmented with the sensor model state equations (7), (8), along with a number of weighting filters. The construction of our robust $H^\infty$ tracking controller is based on the model shown in Figure 7.

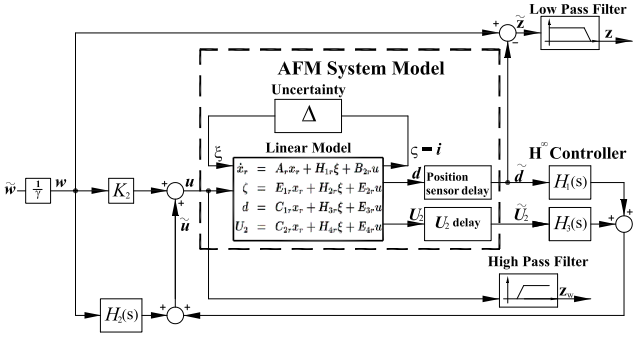


Fig. 7. Block diagram illustrating the robust $H^\infty$ tracking control problem formulation for the AFM positioning system.

We introduce a low pass weighting filter after the error output $\widetilde{z} = w - \widetilde{d}$, and a high pass filter as a weight on the control input. In this robust $H^\infty$ control problem, $\widetilde{w}$ is the normalized reference input and $z$ is the error output. Also, a feed-forward gain $K_2 = 1$ is introduced to represent the default open loop control. The low pass filter on $\widetilde{z}$ has been introduced since no tracking is required at very high frequencies. The low pass filter is chosen to have a transfer function $G_f(s) = \frac{G_f}{s+p_f} = \frac{132\times10^3}{s+3\times10^3}$. A state space model for this low pass filter is obtained as follows:

$$\begin{aligned} \dot{x}_f &= A_f\, x_f + B_f\, \widetilde{z}; \\ z &= C_f\, x_f. \end{aligned} \tag{15}$$

Also, the high pass filter weighting the high frequency inputs is chosen as $G_w(s) = \frac{G_w\, s}{s+p_w} = \frac{1.1\, s + 1.1\times10^{-10}}{s+5000}$. A corresponding state space model for the high pass filter is obtained as follows:

$$\begin{aligned} \dot{x}_w &= A_w\, x_w + B_w\, u; \\ z_w &= C_w\, x_w + D_w\, u. \end{aligned} \tag{16}$$

As mentioned above, the two time delay models (7) and (8) also need to be included in the overall model to allow for

the delay in the outputs $d$ and $U_2$ respectively. Accordingly, the robust $H^\infty$ control problem including the low pass filter, the high pass filter, the position sensor time delay transfer function (7), and the $U_2$ measurement time delay (8) can be defined by the following state equations which also includes extra disturbance inputs to meet the requirements of a standard $H^\infty$ control problem:

$$\dot{x} = \begin{bmatrix} A_r & 0 & 0 & 0 & 0 & 0 \\ -B_f D_d C_{1r} & A_f & B_f C_d & 0 & 0 & B_f C_{f2} \\ B_s C_{1r} & 0 & A_s & 0 & 0 & 0 \\ B_d C_{2r} & 0 & 0 & A_d & 0 & 0 \\ 0 & 0 & 0 & 0 & A_w & 0 \\ 0 & 0 & 0 & 0 & 0 & A_{f2} \end{bmatrix} x + \begin{bmatrix} H_{1r} \\ B_f D_s H_{3r} \\ B_s H_{3r} \\ B_d H_{4r} \\ 0 \\ 0 \end{bmatrix} \xi + \begin{bmatrix} \frac{K_2 B_{2r}}{\gamma} & 0 & 0 & 0 \\ \frac{-K_2 B_f D_s E_{3r}}{\gamma} & 0 & 0 & 0 \\ \frac{K_2 B_s E_{3r}}{\gamma} & 0 & 0 & 0 \\ \frac{K_2 B_d E_{4r}}{\gamma} & 0 & 0 & 0 \\ \frac{K_2 B_w}{\gamma} & 0 & 0 & 0 \\ \frac{B_{f2}}{\gamma} & 0 & 0 & 0 \end{bmatrix} \breve{w} + \begin{bmatrix} B_{2r} \\ B_f D_s E_{3r} \\ B_s E_{3r} \\ B_d E_{4r} \\ B_w \\ 0 \end{bmatrix} \widetilde{u};$$

$$\zeta = \begin{bmatrix} E_{1r} & 0 & 0 & 0 & 0 & 0 \end{bmatrix} x + H_{2r}\,\xi + \begin{bmatrix} \frac{K_2 E_{2r}}{\gamma} & 0 \end{bmatrix} \bar{w} + E_{2r}\widetilde{u};$$

$$\breve{z} = \begin{bmatrix} 0 & C_f & 0 & 0 & 0 & 0 \\ 0 & 0 & 0 & 0 & C_w & 0 \end{bmatrix} x + \begin{bmatrix} 0 \\ 0 \end{bmatrix} \xi + \begin{bmatrix} 0 & 0 & 0 & 0 \\ \frac{D_w K_2}{\gamma} & 0 & 0 & 0 \end{bmatrix} \breve{w} + \begin{bmatrix} 0 \\ D_w \end{bmatrix} \widetilde{u};$$

$$\overline{y} = \begin{bmatrix} D_d C_{1r} & 0 & C_s & 0 & 0 & 0 \\ 0 & 0 & 0 & 0 & 0 & 0 \\ D_d C_{2r} & 0 & 0 & C_d & 0 & 0 \end{bmatrix} x + \begin{bmatrix} D_s H_{3r} \\ 0 \\ D_d H_{4r} \end{bmatrix} \xi + \begin{bmatrix} \frac{D_s H_{3r}}{\gamma} & \epsilon_1 & 0 & 0 \\ \frac{1}{\gamma} & 0 & \epsilon_2 & 0 \\ \frac{K_2 E_{4r} D_d}{\gamma} & 0 & 0 & \epsilon_3 \end{bmatrix} \breve{w} + \begin{bmatrix} D_s E_{3r} \\ 0 \\ D_d E_{4r} \end{bmatrix} \widetilde{u}. \quad (17)$$

Here, $\xi = \Delta(x)\,\zeta, \|\Delta(x)\| \leq 1$, and

$$x = \begin{bmatrix} x_r \\ x_f \\ x_s \\ x_d \\ x_w \\ x_{f2} \end{bmatrix};\ \overline{y} = \begin{bmatrix} \tilde{d} \\ \tilde{w} \\ \tilde{U}_2 \end{bmatrix};\ \breve{w} = \begin{bmatrix} \widetilde{w} \\ w_1 \\ w_2 \\ w_3 \end{bmatrix};\ \breve{z} = \begin{bmatrix} z \\ z_w \end{bmatrix};$$
$$u = \widetilde{u} + K_2\, w.$$

Furthermore, $\widetilde{w}$ is related to the reference input $w$ via the relationship $w = \frac{\widetilde{w}}{\gamma}$, and $w_1$, $w_2$ and $w_3$ are additional disturbances which act as measurement noises in the measurement of the displacement output $\tilde{d}$, the external capacitance output voltage $\tilde{U}_2$ and the reference input signal $w$ respectively. These disturbances are scaled by factors of $\epsilon_1$, $\epsilon_2$ and $\epsilon_3$ which are used as the design parameters in the controller design. The values of these design parameters are adjusted to achieve the best performance in the tracking controller. Also $\breve{z}$ is the error output of the system which has components $z$ and the weighted input signal $z_w$ which is used to provide a penalty on the control input $u$. The additional disturbances $w_1$, $w_2$ and $w_3$ and the addition error output term have been added to ensure that the resulting $H^\infty$ control problem is a standard problem which can be solved using a Riccati equation approach. The parameter $\gamma > 0$ is a design parameter which determines the required level of disturbance attenuation.

### C. Construction of the robust $H^\infty$ controller

We now construct a robust $H^\infty$ controller by applying the results of [17] to the uncertain system defined by the equation (17). This leads us to consider a standard $H^\infty$ problem. Indeed the method of [17], when applied to the uncertain system (18) leads to an $H^\infty$ control problem defined by the state equations:

$$\dot{x} = \underbrace{\begin{bmatrix} A_r & 0 & 0 & 0 & 0 & 0 \\ -B_f D_d C_{1r} & A_f & B_f C_d & 0 & 0 & B_f C_{f2} \\ B_s C_{1r} & 0 & A_s & 0 & 0 & 0 \\ B_d C_{2r} & 0 & 0 & A_d & 0 & 0 \\ 0 & 0 & 0 & 0 & A_w & 0 \\ 0 & 0 & 0 & 0 & 0 & A_{f2} \end{bmatrix}}_{\bar{A}} x + \underbrace{\begin{bmatrix} \sqrt{\epsilon} H_{1r} & \frac{K_2 B_{2r}}{\gamma} & 0\ 0\ 0 \\ -\sqrt{\epsilon} B_f D_s H_{3r} & \frac{-K_2 B_f D_s E_{3r}}{\gamma} & 0\ 0\ 0 \\ \sqrt{\epsilon} B_s H_{3r} & \frac{K_2 B_s E_{3r}}{\gamma} & 0\ 0\ 0 \\ \sqrt{\epsilon} B_d H_{4r} & \frac{K_2 B_d E_{4r}}{\gamma} & 0\ 0\ 0 \\ 0 & \frac{B_w K_2}{\gamma} & 0\ 0\ 0 \\ 0 & \frac{B_{f2}}{\gamma} & 0\ 0\ 0 \end{bmatrix}}_{\bar{B}_1} \bar{w} + \underbrace{\begin{bmatrix} B_{2r} \\ B_f D_s E_{3r} \\ B_s E_{3r} \\ B_d E_{4r} \\ B_w \\ 0 \end{bmatrix}}_{\bar{B}_2} \widetilde{u}$$

$$\begin{bmatrix} \zeta \\ z \\ z_w \end{bmatrix} = \underbrace{\begin{bmatrix} \frac{E_{1r}}{\sqrt{\epsilon}} & 0 & 0 & 0 & 0 & 0 \\ 0 & C_f & 0 & 0 & 0 & 0 \\ 0 & 0 & 0 & 0 & C_w & 0 \end{bmatrix}}_{\bar{C}_1} x + \underbrace{\begin{bmatrix} H_{2r} & \frac{K_2 E_{2r}}{\sqrt{\epsilon}\gamma} & 0\ 0\ 0 \\ 0 & 0 & 0\ 0\ 0 \\ 0 & \frac{D_w K_2}{\gamma} & 0\ 0\ 0 \end{bmatrix}}_{\bar{D}_{11}} \bar{w} + \underbrace{\begin{bmatrix} \frac{E_{2r}}{\sqrt{\epsilon}} \\ 0 \\ D_w \end{bmatrix}}_{\bar{D}_{12}} \widetilde{u};$$

$$\begin{bmatrix} \hat{d} \\ \hat{w} \\ \hat{U}_2 \end{bmatrix} = \underbrace{\begin{bmatrix} D_s C_{1r} & 0 & C_s & 0 & 0 & 0 \\ 0 & 0 & 0 & 0 & 0 & 0 \\ D_d C_{2r} & 0 & 0 & C_d & 0 & 0 \end{bmatrix}}_{\bar{C}_2} +$$
$$\underbrace{\begin{bmatrix} \sqrt{\epsilon} D_s H_{3r} & \frac{K_2\, E_{3r} D_s}{\gamma} & \epsilon_1 & 0 & 0 \\ 0 & \frac{1}{\gamma} & 0 & \epsilon_2 & 0 \\ \sqrt{\epsilon} D_d H_{4r} & \frac{K_2\, E_{4r} D_d}{\gamma} & 0 & 0 & \epsilon_3 \end{bmatrix}}_{\bar{D}_{21}} \bar{w} + \underbrace{\begin{bmatrix} D_s E_{3r} \\ 0 \\ D_d E_{4r} \end{bmatrix}}_{\bar{D}_{22}} \widetilde{u}. \quad (18)$$

Here, $\epsilon > 0$ is an additional design parameter introduced according to the theory of [17] and [18]. In this $H^\infty$ control problem, it is required to construct an output feedback controller such that the closed loop system is stable and the transfer function from $\bar{w}$ to $\bar{z}$ has $H^\infty$ norm strictly less than one.

However, the $H^\infty$ control problem defined by the state equations (18) is not a standard $H^\infty$ problem since the $\bar{D}_{11}$ term is non-zero. This means that the standard Riccati equation approach cannot be applied directly to this problem. Hence, we now apply a standard loop shifting method to remove the $\bar{D}_{11}$ term; see also Section 4.5.1 of [22]. Indeed, we consider a $H^\infty$ control problem defined by the state equations of the form:

$$\begin{aligned} \dot{x} &= \bar{A}x + \bar{B}_1\bar{w} + \bar{B}_2\widetilde{u}; \\ z &= \bar{C}_1 x + \bar{D}_{11}\bar{w} + \bar{D}_{12}\widetilde{u}; \\ y &= \bar{C}_2 x + \bar{D}_{21}\bar{w} + \bar{D}_{22}\widetilde{u}. \end{aligned} \quad (19)$$

where we assume $\bar{D}_{11}'\bar{D}_{11} < I$, and we wish to construct an output feedback controller such that the closed loop system is stable and the $H^\infty$ norm of the closed loop transfer function from $w$ to $z$ is strictly less than unity. In order to achieve this, the condition $\Theta = I - \bar{D}_{11}'\bar{D}_{11} > 0$ must hold. Then, in order to remove the $\bar{D}_{11}$ term, we define $\breve{w} = \Theta^{\frac{1}{2}}\bar{w} - \Theta^{-\frac{1}{2}}\bar{D}_{11}'(\bar{C}_1 x + \bar{D}_{12}u)$ and $\Psi = I + \bar{D}_{11}\Theta^{-1}\bar{D}_{11}' > 0$. From this it follows that this $H^\infty$ control problem is equivalent to an $H^\infty$ control problem defined by the state equations

$$\begin{aligned} \dot{x} &= \widetilde{A}x + \widetilde{B}_1\breve{w} + \widetilde{B}_2\widetilde{u}; \\ \bar{z} &= \widetilde{C}_1 x + \widetilde{D}_{12}\widetilde{u}; \\ \overline{y} &= \widetilde{C}_2 x + \widetilde{D}_{21}\breve{w} + \widetilde{D}_{22}\widetilde{u}. \end{aligned} \quad (20)$$

where, $\tilde{A} = \bar{A}+\bar{B}_1\Theta^{-1}\bar{D}'_{11}\bar{C}_1$; $\tilde{B}_1 = \bar{B}_1\Theta^{\frac{1}{2}}$;
$\tilde{B}_2 = \bar{B}_2+\bar{B}_1\Theta^{-1}\bar{D}'_{11}\bar{D}_{12}$; $\tilde{C}_1 = \Psi^{\frac{1}{2}}\bar{C}_1$;
$\tilde{C}_2 = \bar{C}_2+\bar{D}_{21}\Theta^{-1}\bar{D}'_{11}\bar{C}_1$; $\tilde{D}_{12} = \Psi^{\frac{1}{2}}\bar{D}_{12}$;
$\tilde{D}_{21} = \bar{D}_{21}\Theta^{-\frac{1}{2}}$; $\tilde{D}_{22} = \bar{D}_{22}+\bar{D}_{21}\Theta^{-1}\bar{D}'_{11}\bar{D}_{12}$

Having removed the $\bar{D}_{11}$ term using above method, the $H^\infty$ control problem defined by the state equations (19) can be converted into a standard $H^\infty$ control problem (20) to be solved via an algebraic Riccati equation approach by adding a new measured output $\breve{y} = \bar{y} - \tilde{D}_{22}\tilde{u}$; e.g., see [19], [20], [21] and [22]. The design parameters used in our case were chosen as shown in Table II.

| | |
|---|---|
| $\epsilon$ | $4.83 \times 10^{-9}$ |
| $\epsilon_1$ | $8.0 \times 10^{-4}$ |
| $\epsilon_2$ | $4.0 \times 10^{-5}$ |
| $\epsilon_3$ | $5.9 \times 10^{-4}$ |
| $\gamma$ | 288 |
| $p_f$ | $3.0 \times 10^3$ rad/s |
| $G_f$ | 44 |
| $p_w$ | $5.0 \times 10^3$ rad/s |
| $z_w$ | $1.0 \times 10^{-10}$ rad/s |
| $G_w$ | 1.1 |

Table II Robust $H^\infty$ controller design parameters.

## V. Performance of the Robust $H^\infty$ Controller

### A. Experimental test setup

The robust $H^\infty$ tracking controller for the AFM positioning system was implemented in the dSpace DSP system as illustrated in Figure 8. The continuous time controller transfer functions obtained above were discretized using a standard zero order hold method with a sampling period of 50 kHz for both the x and y directions.

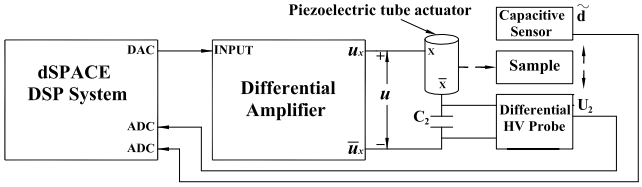


Fig. 8. Experimental test setup used in the AFM positioning system.

### B. Frequency domain performance of the Robust $H^\infty$ control system

The robust $H^\infty$ controller was synthesized to yield the controller transfer functions $H_1(s)$, $H_2(s)$ and $H_3(s)$, in which $H_1(s)$ and $H_3(s)$ are connected as a feedback to the plant outputs $d$ and $U_2$ respectively, and $H_2(s)$ is connected as a feedforward to the reference input $w$. Bode plots of $H_1(s)$, $H_2(s)$, $H_3(s)$ are shown in Figures 9 - 11.

From these Bode plots, it can be seen that our $H^\infty$ control method has yielded a controller with reasonable gains and bandwidth. In order to verify the stability of the resulting control system, a Nyquist plot of the loop gain frequency response is presented in Figure 12. In this Nyquist plot, the loop gain frequency response data is obtained by multiplying the measured open loop plant frequency response data by the calculated controller frequency response of each frequency. This Nyquist plot indicates that the control system should indeed be robustly stable.

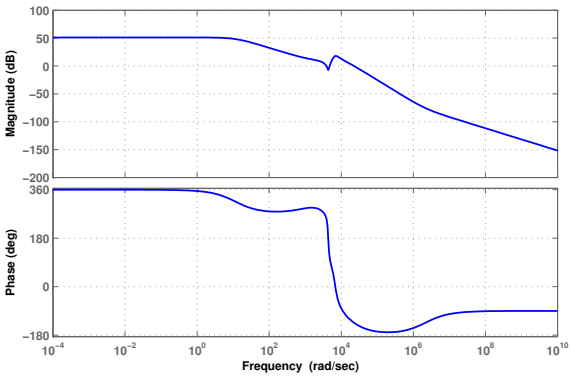


Fig. 9. Bode plot of the controller transfer function $H_1(s)$ from $\tilde{d}$ to $\tilde{u}$.

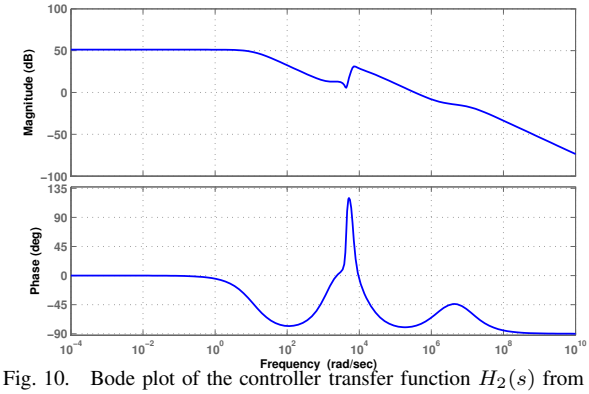


Fig. 10. Bode plot of the controller transfer function $H_2(s)$ from $\widehat{w}$ to $\tilde{u}$.

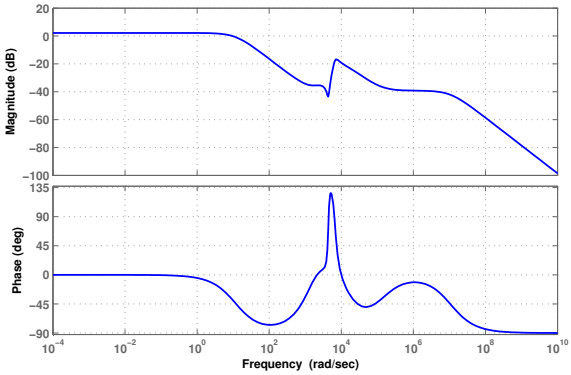


Fig. 11. Bode plot of the controller transfer function $H_3(s)$ from $\tilde{U}_2$ to $\tilde{n}$

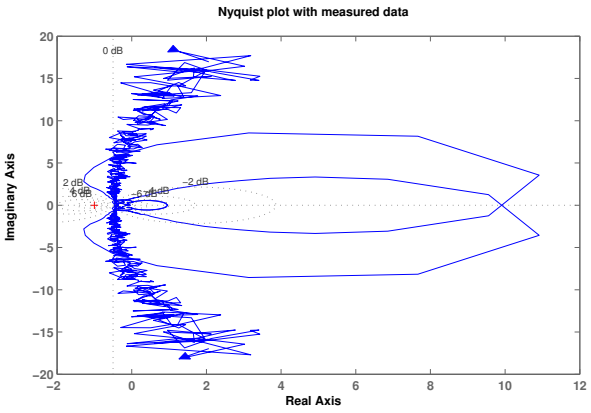


Fig. 12. Nyquist plot of the loop gain frequency response using the measured data.

In the closed-loop case, four different Bode plots are given. The first of these plots corresponds to the frequency response of the measured closed-loop frequency response. The second of these plots corresponds to the closed-loop frequency response calculated using the measured open loop frequency response data. The third of these plots corresponds to the frequency response calculated from the plant and our controller models. The fourth of these plots corresponds to the measured open loop frequency response.

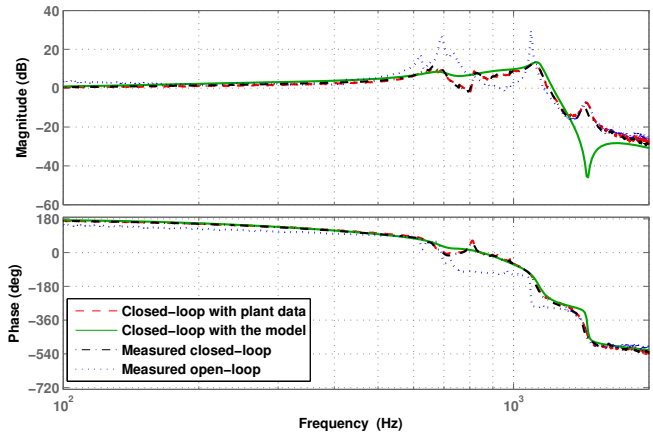


Fig. 13. A comparison of Bode plots for the open loop and closed loop transfer functions.

### C. Experimental tracking performance of the robust $H^\infty$ control system

The performance of the robust $H^\infty$ controller was also examined experimentally by tracking a sawtooth reference signal applied to the piezoelectric tube actuator. The frequency of the reference sawtooth input signal is set at 5 Hz, see Figure 14

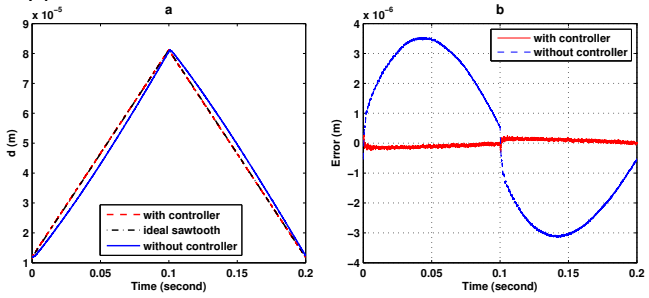


Fig. 14. (a) Displacement signal with a 5Hz sawtooth reference input $w$. (b) tracking error with 5Hz reference input.

## VI. Image Scanning Results

### A. Low pass filtering at the reference signal

The robust $H^\infty$ controller designed for the AFM positioning system has a much higher bandwidth than the original PID controller. When this controller was implemented it was found that abrupt change in the reference signals lead to significant oscillations in the tube scanner resulting in poor image qualities. Hence, we introduced Chebychev low pass filters on the reference signals with different cut-off frequencies in the x and y directions. The best cut-off frequencies used for the x and y directions were 900Hz and 100Hz respectively.

### B. Scanned images

Using the existing NT-MDT AFM scanning software, any scanning speed above 10Hz can only be set to frequencies of 10Hz, 31.25Hz, 62.5Hz and 125Hz. Figures 15 to 18 illustrate the results obtained using our robust $H^\infty$ tracking controller implemented in a dSpace DSP control system to control the AFM scanning system in both x and y directions compared to the internal PID controller. Each of these images was obtained by scanning a TGQ1 grating reference sample.

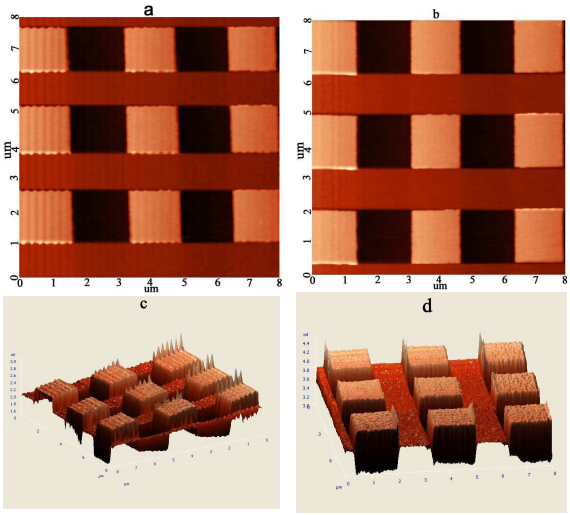


Fig. 15. 10Hz scanned images using the AFM PID controller (a) 2D-image (c) 3D-image and using the $H^\infty$ controller (b) 2D-image (d) 3D-image.

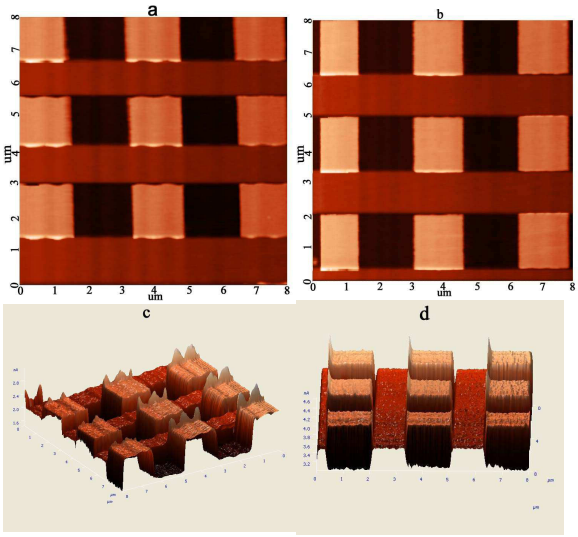


Fig. 16. 31.25Hz scanned images using the AFM PID controller (a) 2D-image (c) 3D-image and using the $H^\infty$ controller (b) 2D-image (d) 3D-image.

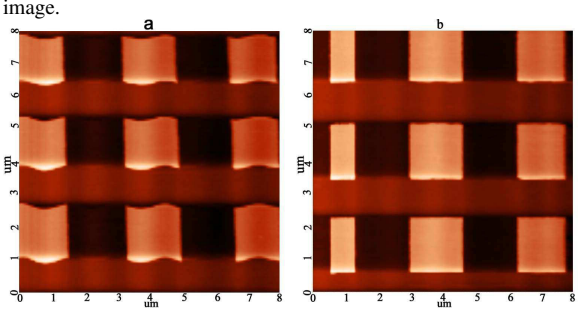

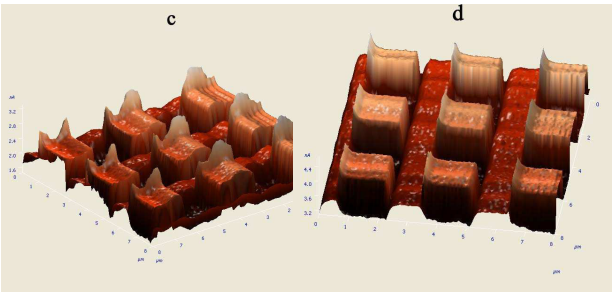


Fig. 17. 62.5Hz scanned images using the AFM PID controller (a) 2D-image (c) 3D-image and using the $H^\infty$ controller (b) 2D-image (d) 3D-image.

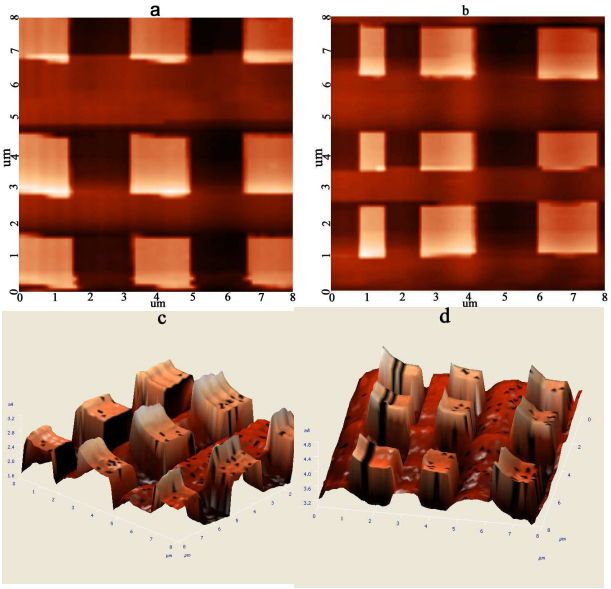


Fig. 18. 125Hz scanned images using the AFM PID controller (a) 2D-image (c) 3D-image and using the $H^\infty$ controller (b) 2D-image (d) 3D-image.

## VII. Conclusion

In this paper, we consider the use of a robust $H^\infty$ tracking controller for fast scanning in Atomic force Microscopy. Experimental results show that high speed and high precision 3D-image scanning can be achieved using our controller. The performance obtained from the scanned images have been compared with the conventional AFM PID control method in our commercial type NT-MDT AFM. A comparison was given in this paper between the use of our robust $H^\infty$ controller and the NT-MDT AFM PID controller and our experimental results showed that the scanned images were significantly improved at scanning speeds of up to $125\,\text{Hz}$. It has been noted that the oscillations occur with the tracking performance for scanning speed above $60\,\text{Hz}$. Therefore, further control strategy is needed for active damping of these oscillations at higher frequencies.

## VIII. Acknowledgment

The authors would like to acknowledge the technical assistance we received during our experimental tests from Mr. Shane Brandon of the School of Engineering and Information Technology, Australian Defence Force Academy.

## References

[1] A. J. Fleming, S. S. Aphale and S. O. R. Moheimani, A new robust damping and tracking controller for SPM position stages. *Proceedings of the American Control Conference*, Louis, MO,USA 2009.

[2] S. Kuiper and G. Schitter, Self-sensing actuation and damping of a piezoelectric tube scanner for atomic force microscopy. *Proceedings of the European Control Conference*, Budapest, Hungary 2009

[3] S. O. R. Moheimani and Y. K. Yong, A new piezoelectric tube scanner for simultaneous sensing and actuation. *Proceedings of the American Control Conference*, Louis, MO, USA 2009

[4] B. Bhikkaji and S. O. R. Moheimani, Intergral resonant control of a piezoactuators tube actuator for fast nanoscale positioning. *IEEE/ASME Transactions on Mechatronics*, Vol.13, No.5, pp. 530-536, 2008.

[5] T. Shiraishi and H. Fujimoto, High-speed high-precision control of atomic force microscope by surface topography learning observer. *Proceedings of the American Control Conference*, Louis, MO, USA 2009.

[6] I. A. Mahmood and S. O. R. Moheimani, Improvement of accuracy and speed of a commercial AFM using positive position feedback control. *Proceedings of the American Control Conference*, Louis, MO, USA 2009

[7] H. Jung, J. Y. Shim and D. Gweon, Tracking control of piezoelectric actuators. *Nanotechnology*, Vol.12(1), pp. 14-20, 2001.

[8] R. Banning, W. de Koning, H. Adriaens and R. Koops, State-space analysis and identification for a class of hysteretic systems. *Automatica*, Vol.37(12), pp. 1883-1892, 2001.

[9] D. Croft, G. Shedd and S. Devasia, Creep, hysteresis, and vibration compensation for piezoactuators: atomic force microscopy application. *Proceedings of the American Control Conference*, Chicago, Illinons, pp. 2123-2128, Jun. 2000.

[10] M. Goldfarb and N. Celanovic, Modeling piezoelectric stack actuators for control of micromanipulation. *IEEE Control Systems Magazine*, Vol.17(3), pp. 69-79, 1997.

[11] A. Sebastian and S. M. Salapaka, Design methodologies for robust nano-positioning. *IEEE Transactions on Control Systems Technology*, Vol.13(6), pp. 868-876, 2005.

[12] M. Salah, M. McIntyre, D. Dawson and J. Wagner, Robust Tracking Control for a Piezoelectric Actuator. *Proceedings of the American Control Conference*, New York, USA, pp. 106-111, Jul. 2007.

[13] S. O. R. Moheimani and B. J. G. Vautier, Resonant control of structural vibration using charge-driven piezoelectric actuators. *IEEE Transactions on Control Systems Technology*, Vol.13(6), pp. 1021-1035, 2005.

[14] A. J. Fleming and K. K. Leang, Evaluation of charge drives for scanning probe microscope positioning stages. *Proceedings of the American Control Conference*, Seattle, Washington, USA, pp. 2028-2033, Jun. 2008.

[15] N. Tamer and M. Dahleh, Feedback control of piezoelectric tube scanners. *Proceeding of the 33rd Conference on Decision and Control*, Lake Buena, FL, USA, 1994.

[16] H. Adriaens, W. de Koning and R. Banning, Modeling piezoelectric actuators. *IEEE/ASME Transactions on Mechatronics*, Vol.5(4), pp. 331-341, 2000.

[17] L. Xie, M. Fu, and C. E. de Souza, Robust $H_\infty$ control and quadratic stabilization of systems with parameter uncertainty via output feedback. *IEEE Transactions on Automatic Control*, Vol.37(8), pp. 1253-1256, 1992.

[18] L. Xie and C. E. de Souza, Robust $H_\infty$ Control for linear systems with norm-bounded Time-varying uncertainty. *IEEE Transactions on Automatic Control*, Vol.37(8), pp. 1188-1191, 1992.

[19] I. R. Petersen, B. D. O. Anderson and E. A. Jonckeere, A first principles solution to the non-singular $H^\infty$ control problem. *International Journal of Robust and Nonlinear Control*, Vol.1(3), pp. 171-185, 1991.

[20] K. Zhou, J. Doyle and K. Glover, Robust and Optimal Control. *Prentice-Hall*, Upper Saddle River, NJ, 1996.

[21] M. Green and D. J. N. Limebeer, Linear Robust Control. *Prentice-Hall*, Englewood Cliffs, NJ, 1995.

[22] T. Baser and P. Bernard, $H^\infty$-Optimal Control and Related Minimax Design Problems: A Dynamic Game Approach, *Birkhäuser*, Boston, 1995.

[23] N. Chuang and I. R. Petersen, Robust $H^\infty$ control of hysteresis in a piezoelectric stack actuator. *IFAC Seoul, South Korea*, 2008

[24] N. Chuang and I. R. Petersen, Robust $H^\infty$ control in nano-positioning. *IEEE MSC Japan*, September 2010